Electronic Supplementary Information for:

K-doped $Sr_2Fe_{1.5}Mo_{0.5}O_{6-\delta}$ predicted as bifunctional catalyst for air electrodes in proton-conducting solid-oxide electrochemical cells

Ana B. Muñoz-García* and Michele Pavone*

Department of Chemical Sciences, University of Naples Federico II, Comp. Univ. Monte Sant'Angelo Via Cintia 26, 80121 Naples, Italy

S.1 Structural models

Intermediate species of the OER/ORR reactions have been modeled with 1x1x9-layer slabs that expose $(Fe_{0.75}Mo_{0.25})O_2$-terminated SFMO/KSFMO (001) surfaces, constructed from the corresponding 40-atom pseudo-cubic cells, which results in $Fe_3Mo_1O_8$ surface supercells (**Figure S1**). This stoichiometry reflects the homogeneous Mo distribution in bulk SFMO. To simulate the maximum effect of the dopant in KSFMO, we have substituted Sr by K at the closest position to the reaction site, i.e. in the subsurface layer. Although they may differ somewhat from those of real electrodes, these model surfaces, compositions and structures help us to deconvolute the electronic and structural effects arising from each transition metal ion (Fe and Mo) and K doping in the perovskite oxide environment.

Adsorbate species (O, OH, OOH, O_2 and H_2O) were introduced on both sides of the slab to avoid net dipole moments (see main text for description of the active sites surveyed). We have considered an antiferromagnetically aligned Fe sub-lattice,[S1] with the central layer as a symmetry plane. Lateral lattice vectors have been set to the theoretically determined equilibrium lattice constants for SFMO and KSFMO (7.87 and 7.92 Å, respectively).[S2] The vacuum layer, considered beyond the adsorbates, is always > 13 Å to avoid interaction between images. In structural optimizations, atom positions of the three outermost layers of each side of the slab and those of the adsorbates have been allowed to relax while the three central layers are frozen and simulate bulk-like structures. We have found that relaxing only the two outermost layers is enough for stoichiometric slabs and for those with Fe-V_O-Fe, but creates an artificial strain when heavily reconstructed Mo-V_O-Fe sites are present (see main text).

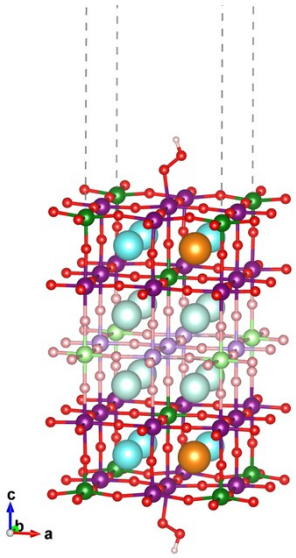

Figure S1. 9-layer slab model for stoichiometric (K)SFMO (001) surface showing a *OOH symmetrically adsorbed to both sides of the slab. Color code: Sr (cyan), K(orange), Fe(purple), Mo(green), O(red), H(light pink). The three central layers are shown in faded colors to indicate that are frozen during geometry optimization.

In order to elucidate whether the strong reconstruction on SFMO and KSFMO surfaces after formation Mo-V_O-Fe –like vacancy is not an artifact of the structural model used, we have performed structural relaxations on 2x2 supercells of the $Sr_{16}Fe_{15}Mo_5O_{56}$ slab (*i.e.* $Sr_{64}Fe_{60}Mo_{20}O_{224}$) containing one surface Mo-V_O-Fe. **Figure S2** shows the relaxed structure of the two slab models. We observe the same pattern (i.e. the tetrahedral-like reconstruction around Mo) for both slabs/vacancy concentrations. The formation energy of this vacancy ($\Delta E_{form}(V_O^{\bullet\bullet})$, see below) in the larger cell is ~ -1.5 eV, which reinforces the picture of (K)SFMO surfaces containing both Fe-V_O-Fe and Mo-V_O-Fe.

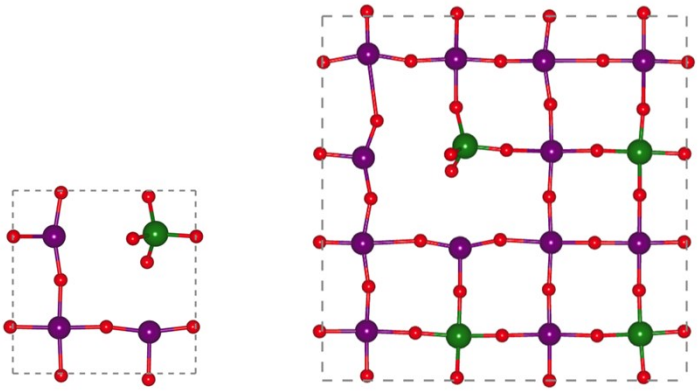

Figure S2. Top view of the relaxed structure of $(Fe_{0.75}Mo_{0.25})O_2$-terminated 1x1x9L (left) and 2x2x9L (right) periodic supercells containing a single vacancy between surface Mo and Fe atoms (Mo-V_O-Fe).

S.2 Computational details

On structures described in section S.1, we have performed DFT[S3] +U [S4] calculations as implemented in the Vienna Ab-Initio Simulation Package (VASP)[S5] to correct for the significant self-interaction error inherent to standard DFT when applied to transition metal oxides with tightly localized *d* electrons. We used the Perdew-Burke-Ernzerhof (PBE)[S6] exchange-correlation functional and an *ab initio*-derived *U-J* value of 4.0 eV[S7] for Fe to account for intra-atomic *d* - *d* Coulomb (*U*) and exchange (*J*) interactions. This PBE+U combination was validated in previous calculations on bulk SFMO and related materials.[S8] Nuclei and core electrons were replaced by projector augmented wave (PAW) potentials obtained from the VASP repository. With the standard PAW potential for oxygen, a plane-wave basis kinetic energy cutoff of 600 eV is required for convergence of the total energy to within 3 meV per formula unit.

Upon removal of symmetric surface oxygen atoms in the slab models described above, the oxygen vacancy formation energy $\Delta E_{form}(V_O^{\bullet\bullet})$ has been calculated from the energies of the stoichiometric (host) and non-stoichiometric (defect) slabs and of the isolated oxygen molecule in its ground triplet state, all calculated at the same level of theory, according to:

$$\Delta E_{form}(V_O^{\bullet\bullet}) = \frac{1}{2}(E_{defect} - E_{host} - \frac{1}{2}E_{O_2(g)}) \qquad \text{Eq. S1}$$

ZPE and entropic contributions are obtained from vibrational frequencies (ω_i), which are determined from the eigenvalues of the Hessian matrix calculated from central finite differences of analytic gradients, where N selected atoms are displaced 0.02 Å along the x, y and z directions. Due to the presence of two active surface TM (Fe and Mo), we have calculated both sets of frequencies, namely those corresponding to Fe-O, Fe-OH, Fe-OOH, Fe-OH_2 and Mo-O, Mo-OH, Mo-OOH, Mo-OH_2 intermediates in SFMO. These moieties, i.e. the active site and the adsorbate correspond to the N selected atoms chosen to calculate ω_i.

The entropic contributions for gaseous molecules are taken from standard thermodynamic tables. We have calculated entropic contributions from adsorbed species from the vibrational partition function

$$S = k_B \ln \prod_{i=1}^{3N} \frac{1}{1 - e^{-(\hbar\omega_i / k_B T)}} \qquad \text{Eq. S2}$$

These contributions are known to be small for Fe active sites in Fe_2O_3 [S9] and are usually omitted [S10] but, to the best of our knowledge, they have not been reported for Mo-containing solids. For completeness, we have calculated them for intermediates attached to both Mo and Fe in SFMO.

The analysis described below is based on purely thermodynamic considerations and overpotentials discussed in this work can be considered as lower bounds for operation overpotentials that arise also from electrochemical kinetic barriers, where determination of rate limiting steps (RDS) is needed besides determining PDS. For this reason, although materials for PC-SOFC/EC applications are intended to work between 400 and 600°C, all results present in this work correspond to the evaluation of the entropic terms at T=298.15K, where the thermodynamic model holds. In this way, we evaluate the intrinsic catalytic effects of a given specific site, which can be directly compared to those of well-studied catalysts and photo-catalysts as Fe_2O_3.[S11] ZPE and entropic contributions are listed for individual species in **Table S1**. The ZPE corrections computed for Fe_2O_3 are included for comparison. Our results show that the ZPE for Fe and Mo are very close. This similarity, found also between Fe_2O_3 and TiO_2, [S12] indicates that vibrational frequencies of O-O and O-H bonds do not change significantly for different metal oxide substrates.

Table S1. ZPE Corrections and Entropic energy contributions for gaseous and adsorbed species on Fe and Mo surface sites of SFMO (001). *Values for Fe_2O_3 from Ref. S10. ** Value for Fe_2O_3 from Ref. S9.

	ZPE (eV)		**$TS_{298.15K}$ (eV)**	
H_2 (g)	0.27		0.40	
O_2 (g)	0.10		0.63	
H_2O (l)	0.57		0.67	
	Fe	**Mo**	**Fe**	**Mo**
***O**	0.05 (0.04*)	0.06	0.01	0.01
***OH**	0.31 (0.37*)	0.31	0.02	0.02
***OOH**	0.42 (0.48*)	0.43	0.05	0.04
***OH_2**	0.65 (0.67*)	0.65	0.04	0.02
***O_2**	0.12 (0.10**)	0.13	0.03	0.05

S.3 OER/ORR overpotential calculation

The OER/ORR reaction mechanisms from water to oxygen plus hydrogen (and vice-versa) involve intermediate species that can be considered as the products of four independent proton-coupled electron transfer (PCET) steps, after initial adsorption of H_2O (or O_2) at the electrode surface:

OER		**ORR**	
$H_2O + * \rightarrow *OH_2$	(E1)	$O_2 + * \rightarrow *OO$	(R1)
$*OH_2 \rightarrow *OH + H^+ + e^-$	(E2)	$*OO + H^+ + e \rightarrow *OOH$	(R2)
$*OH \rightarrow *O + H^+ + e^-$	(E3)	$*OOH + H^+ + e \rightarrow *O + H_2O$	(R3)
$*O + H_2O \rightarrow *OOH + H^+ + e^-$	(E4)	$*O + H^+ + e^- \rightarrow *OH$	(R4)
$*OOH \rightarrow * + O_2 + H^+ + e^-$	(E5)	$*OH + H^+ + e^- \rightarrow * + H_2O$	(R5)

Formation/dissociation of O_2 from/to two *O (after steps E3/R2 in OER/ORR) could in principle be possible, but it has been shown that this route has high activation energies and high overpotentials,[S13] so we have explored the more widely accepted non-associative/non-dissociative mechanism for the OER/ORR, which involves surface *OOH species as depicted by **Figure S3**.

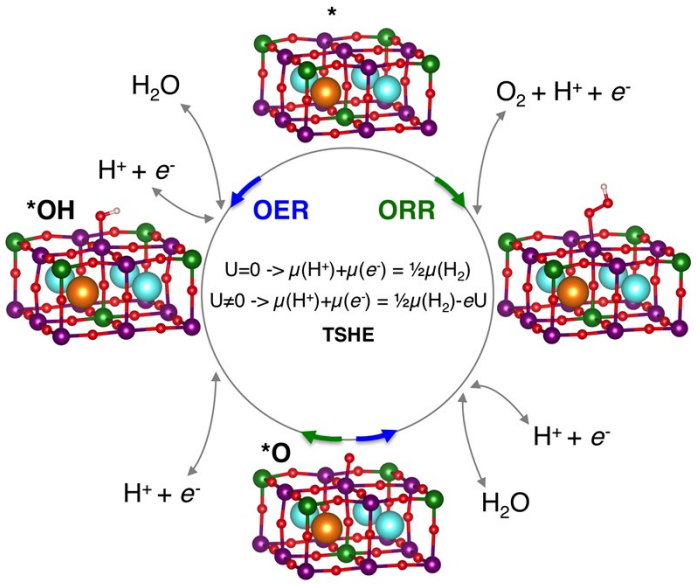

Figure S3. Schematic illustration of the water oxidation / oxygen reduction reaction pathways through four proton-coupled electron transfer steps.

To calculate the free energy of each step, we have adopted the theoretical standard hydrogen electrode (TSHE) scheme introduced by Nørskov and co-workers, [S14] where one can obtain the energy of H^++e^- couple by referencing it to the energy of the H_2 molecule using the standard hydrogen electrode (SHE, p=1atm, T=298K, pH=0):

$$\mu(H^+)+\mu(e^-)=\frac{1}{2}\mu(H_2) \quad \text{for U=0}$$

The chemical potential of electrons and protons change in the presence of an external bias U (against SHE) as:

$$\mu(H^+)+\mu(e^-)=\frac{1}{2}\mu(H_2)-eU \quad \text{for U}\neq 0$$

Therefore, free energies of PCET steps can be computed as a function of U according to:

$$\Delta G(U) = \Delta E + (\Delta ZPE - T\Delta S) - eU$$

where ΔE is the reaction energy, computed from the electronic energies of the reaction intermediates (*O, *OOH, *OH, $*O_2$, $*OH_2$) and the energies of the H_2, O_2 and H_2O molecules, ΔZPE is the zero-point vibrational energy change and ΔS is the entropy change. $\Delta ZPE - T\Delta S$ variations for reaction steps E1-E5/R1-R5 computed from results in Table S1 are presented in **Table S2**.

Table S2. ZPE and Entropic energy corrections for reaction steps E1-E5 and R1-R5 on Fe and Mo sites of SFMO (001).

		ΔZPE-TΔS (eV)	
		Fe	**Mo**
OER	**E1**	+0.71	+0.73
	E2	-0.38	-0.41
	E3	-0.32	-0.31
	E4	+0.37	+0.37
	E5	-0.98	-0.99
ORR	**R1**	+0.63	+0.62
	R2	+0.34	0.37
	R3	-0.37	-0.37
	R4	+0.32	+0.31
	R5	-0.32	-0.32

At U=0, steps E2-E5 for the OER are uphill, while R2-R5 are downhill, with positive and negative overall ΔG, respectively. According to Nørskov et al., we define the onset potentials U_{OER}/U_{ORR} as the external bias that makes all E2-E5 and R2-R5 steps downhill (ΔG≤0). U_{OER} corresponds to the minimum potential that needs to be applied to carry out the otherwise thermodynamically unfavorable OER, while U_{ORR} corresponds to the maximum possible potential delivered by the cell in the ORR process. The theoretical overpotentials (η_{OER} and η_{ORR}) can be therefore defined then as the difference between U_{OER}/U_{ORR} and E_0 for reaction:

$$H_2O <=> ½\ H_2 + O_2$$

which is experimentally 1.23 V in the electrolysis cell. With no applied potential (U=0), calculated ΔG for the overall OER reaction at the DFT-PBE level of theory is 4.44 eV. The predicted electrochemical potential per PCET is then E_0(DFT-PBE) = 4.44/4e^- = 1.11 V, a value in reasonable agreement with measured value of 1.23 V. The slight difference comes from to the well-known drawbacks of DFT on describing the O_2 molecule[S15] and from the use of harmonic frequencies. Some authors use the experimental E_0 value (and the experimental value for the total energy of the O_2 molecule) [S9, S16] to calculate the theoretical overpotential, while others use E_0(DFT). [S10, S17] We adopted the latter since the differences are very small and do not change qualitatively nor quantitatively the results present in this study.

We computed the overpotential (in V) as:

$$\eta_{OER} = (\Delta G_{max}^{E2\text{-}E5}/e^-) - 1.11 \qquad \text{(Eq. S3)}$$

$$\eta_{ORR} = 1.11 - (|\Delta G_{min}^{R2\text{-}R5}|/e^-) \qquad \text{(Eq. S4)}$$

for the OER and ORR, respectively. The step that delivers ΔG_{max}(ΔG_{min}) along the OER(ORR) mechanism will be, therefore, the potential determining step (PDS). Analyzing onset and overpotential dependence on pH is not trivial and is out of the scope of this paper but, since ΔG of Eqs. E2-E5 and R2-R5 vary in the same way with pH, the PDS remains the same.[S18] Calculated ΔG of steps E1-E5 and R1-R5 are given in **Table S3**.

Table S3. Free Energies of reactions E1-E5/R1-R5 (ΔG_{298}, in eV) without external bias. ΔG of the PDS for each site highlighted in bold.

		SFMO						KSFMO								
		S1	**S2**	**S3**	**S4**	**S5**	**S6**	**K1**	**K2**	**K3**	**K4**	**K4'**	**K5**	**K6**	**K5'**	**K6'**
O E R	**E1**	0.21	0.21	0.12	0.19	0.28	0.26	0.19	0.20	0.08	0.12	0.22	0.11	0.15	0.16	0.20
	E2	1.79	1.82	1.18	0.62	1.31	1.19	1.99	1.83	1.48	0.82	0.63	1.30	1.43	1.20	**1.70**
	E3	**2.13**	**2.17**	1.24	**1.95**	**2.32**	**2.11**	**2.12**	**2.25**	1.31	**1.96**	**1.91**	0.77	1.28	**2.40**	1.29
	E4	0.88	0.84	**2.20**	1.55	0.81	1.11	0.82	0.73	**1.97**	1.52	1.45	**2.45**	**1.48**	0.89	1.39
	E5	-0.58	-0.60	-0.30	0.14	-0.29	-0.24	-0.69	-0.57	-0.41	0.02	0.22	-0.19	0.10	-0.22	-0.06
O R R	**R1**	0.55	0.55	0.62	0.52	0.50	0.48	0.59	0.59	0.55	0.45	0.47	0.49	0.47	0.49	0.51
	R2	**0.03**	**0.05**	**-0.32**	**-0.66**	**-0.21**	**-0.24**	**0.10**	**-0.02**	**-0.14**	**-0.47**	**-0.69**	**-0.30**	**-0.57**	**-0.27**	**-0.44**
	R3	-0.88	-0.84	-2.20	-1.54	-0.81	-1.10	-0.82	-0.73	-1.97	-1.52	-1.45	-2.45	-1.48	-0.89	-1.39
	R4	-2.13	-2.17	-1.24	-1.95	-2.32	-2.11	-2.12	-2.25	-1.31	-1.96	-1.91	-0.77	-1.28	-2.40	-1.29
	R5	-2.00	-2.03	-1.30	-0.80	-1.59	-1.45	-2.18	-2.03	-1.56	-0.93	-0.85	-1.40	-1.57	-1.35	-1.82

S.3 Electronic structure features of SFMO/KFMO surface active sites

Table S4. Magnetic moments and Bader Charges [S19] of Reaction sites M (M=Fe, Mo or 2xFe for Fe-V_O-Fe vacancies)

	SFMO						KSFMO								
	S1	**S2**	**S3**	**S4**	**S5**	**S6**	**K1**	**K2**	**K3**	**K4**	**K4'**	**K5**	**K6**	**K5'**	**K6'**
M	**Fe**	**Fe**	**Mo**	**Fe (2x)**	**Fe**	**Fe**	**Fe**	**Fe**	**Mo**	**Fe (2x)**	**Fe (2x)**	**Fe**	**Fe**	**Fe**	**Fe**
$\lvert\mu_M\rvert$ (μB)	3.82	4.12	0.10	4.00 4.00	4.14	4.01	3.51	4.10	0.08	4.02 3.81	4.00 3.94	4.09	3.58	4.10	3.66
q (e^-)	+1.77	+1.65	+2.30	+1.60 +1.66	+1.67	+1.59	+1.73	+1.68	+2.41	+1.60 +1.69	+1.61 +1.70	+1.60	+1.78	+1.59	+1.77

References

S1. Muñoz-García, A. B.; Pavone, M.; Ritzmann, A. M.; Carter, E. A. Phys. Chem. Chem. Phys. 2013, 15, 6250−6259.
S2. Muñoz-García, A. B.; Pavone, M.; Chem. Mater. 2016, 28, 490-500.
S3. Kohn, W.; Sham, L. J. Phys. Rev. 1965, 140, A1133− A1138.
S4. Anisimov, V. I.; Aryasetiawan, F.; Lichtenstein, A. I. J. Phys.: Condens. Matter 1997, 9, 767−808.
S5. Kresse, G.; Furthmüller, J. Phys. Rev. B 1996, 54, 11169−11186.
S6. Perdew, J. P.; Burke, K.; Ernzerhof, M. Phys. Rev. Lett. 1996, 77, 3865−3868.
S7. Mosey, N. J.; Liao, P.; Carter, E. A. J. Chem. Phys. 2008, 129, 014103.
S8. Muñoz-García, A. B.; Pavone, M.; Carter, E. A. Chem. Mater. 2011, 23, 4525−4536.
S9. Hellman, A.; Pala, R. G. S. J. Phys. Chem. C 2011, 115, 12901-12907.
S10. Liao, P.; Keith, J. A.; Carter, E. A. J. Am. Chem. Soc. 2012, 134, 13296-13309.
S11. Nguyen, M.-T.; Piccinin, S.; Seriani, N.; Gebauer, R. ACS Catal. 2015, 5, 715-721.
S12. Valdés, A.; Qu, Z.; Kroes, G.-J.; Rossmeisl, J.; Nørskov, J. K.; J. Phys. Chem. C 2008, 112, 9872-9879.
S13. Rossmeisl, J.; Qu, Z.-W.; Zhu, H.; Kroes, G.-J.; Nørskov, J. K. J. Electroanal. Chem. 2007, 607, 83-89.
S14. Nørskov, J. K.; Rossmeisl, J.; Logadottir, A.; Lindqvist, L.; Kitchin, J. R.; Bligaard, T.; Jónsson, H. J. Phys. Chem. B 2004, 108, 17886-17892.
S15. Wang, L.; Maxisch, T.; Ceder, G. Phys. Rev. B 2006, 73, 195107.
S16. Viswanathan, V.; Hansen, H. A.; Rossmeisl, J. Nørskov, J. K. ACS Catal. 2012, 2, 1654-1660.
S17. Fidelsky, V.; Toroker, M. C. Phys. Chem. Chem. Phys. 2017, 19, 7491-7497.
S18. Valdés, A.; Brillet, J.; Grätzel, M.; Gudmundsdottir, H.; Hansen, H.A.; Jónsson, H.; Klüpfel, P.; Kroes, G.-J.; LeFormal, F.; Man, I.C.; Martins, R. S.; Nørskov, J. K.; Rossmeisl, J.; Sivula, K.; Vojvodic, A.; Zach, M. Phys. Chem. Chem. Phys. 2012, 14, 49-70.
S19. Tang, W.; Sanville, E.; Henkelman, G. J. Phys.: Condens. Matter 2009, 21, 084204.